Modeling and Control of Piezoelectric Hysteresis: A Polynomial-Based Fractional Order Disturbance Compensation Approach

***Abstract*—The performance of piezoelectric nanopositioners is greatly affected by their hysteretic behaviors. However, the hysteresis nonlinearity is difficult to be precisely modeled and compensated for, primarily due to the asymmetric, rate and input amplitude dependent characteristics. This paper proposes a novel method to deal with this challenge. Specifically, a polynomial-based fractional order disturbance model is proposed to accommodate and characterize the complex hysteresis. In this model, the rate dependency is captured by a general method of implementing curve fitting in Bode magnitude plot. Moreover, the inverse model for control purposes is immediately available from the original one. The proposed method does not require expensive computational resources. In fact, this paper shows that this controller can be easily implemented in an analog manner, which brings the advantages of high-bandwidth and low-cost. Extensive modeling and tracking experiments are carried out to demonstrate the effectiveness of the proposed method. It is shown that the piezoelectric hysteresis nonlinearity can be significantly suppressed over a wide bandwidth.**

***Index Terms*—Asymmetric disturbance modeling, fractional order compensator, hysteresis nonlinearity, piezoelectric actuator (PEA), rate-dependent effect.**

NOMENCLATURE

α	Amplitude coefficient of controller input
α_1	Amplitude-varying gain of ascending disturbance
α_2	Amplitude-varying gain of descending disturbance
β	Order of fractional order compensator
$\hat{d}$	Estimated disturbance
$\hat{p}$	Identified polynomial
$\hat{y}$	Estimated displacement
$\tilde{y}$	Reference displacement
A	Amplitude of sinusoidal disturbance model
d	Measured disturbance
e_{rms}	Root-mean-square error
K	Optimal gain between the basis polynomial and the identified polynomial
x	Controller input
y	Measured displacement

I. INTRODUCTION

PIEZO-actuated nano-positioning systems have been widely used in ultra-precision machines and instruments, such as ultrasonic motors [1], lithography systems [2], active optics [3], scanning probe microscopy [4] and robotics [5]. Their desirable positioning capability at the nanoscale not only enables complex functional nanostructures to be created, but also leads to profound understanding of novel phenomenon at the bottom [6]. Generally, a piezo-actuated positioning system utilizes flexure-based mechanism, which is free of friction and wear, to guide the motion of the actuator. The key element of such system is the so-called piezoelectric actuator (PEA) having a number of advantages like microsecond level response time, high stiffness (more than $10^6 N/m$) and sub-nanometer resolution. However, the main disadvantages associated with the PEAs are creep and hysteresis effects. The former appears at low-frequency range and can be easily addressed. While the latter exists between the applied electric field and the resultant mechanical strain over the full bandwidth. As a result, although having an excellent resolution, the motion accuracy of piezo-actuated positioning system is dramatically degraded.

Considering that the origins and mechanisms of the piezoelectric hysteresis are complex, in practice most attentions have been paid on proposing effective control strategies to mitigate this effect. The most straightforward method is probably to integrate precise position sensor into the system and design specific controllers [7]. Other more advanced methods include linear quadratic gaussian control [8], robust adaptive control [9] and learning-based control [10], etc. The advantages of feedback control method lie in its capability of handling the modeling errors, environmental disturbances and parameter variations resulting from the aging and heating issues. However, the high frequency tracking performance of feedback control method is limited by the phase lag from the controller itself and the power amplifier, which can even lead to instability. Moreover, the noise introduced by the position sensor becomes significant at high frequencies, thus degrading the tracking resolution to a large extent. In fact, it is not guaranteed that the closed-loop control performance would be always better than its open-loop counterpart.

Another intuitive method of compensating hysteresis effects is to thoroughly characterize the hysteretic nonlinearity by developing proper mathematical models. The control signal can then be obtained by finding the analytical inversion (or equivalent inversion) of the used model. This is the basic idea of feedforward control. The developed hysteresis models can roughly be grouped into two classes: physics-based models and phenomenological-based models. Physics-based models are built by using first principles of physics [11], in which the Jiles-Atherton model might be the most popular one [12]. On the other hand, phenomenological models including differential equation based models [13]–[15], operator-based models [16] and intelligent hysteresis models [17] have been the focus of feedforward control. The challenges of phenomenological model based method are mainly from the asymmetry, rate and amplitude dependent features of the hysteresis. To precisely describe these features, modification of existing models are usually necessary [18], which significantly increase the model complexity and the required computational resources. These are primary reasons why many of the aforementioned models have not been used in high-bandwidth tracking applications, such as high-speed atomic force microscopy. In fact, the hysteresis compensation for high-bandwidth nanopositioning is a critical yet still open issue, since most of feedback and feedforward control methods cannot provide a satisfactory performance, due to the above-mentioned reasons.

In addition, it is also worth mentioning that charge control approach [19] [20] is a special case of feedforward control, which could be a promising solution for real practice. This method can effectively suppress piezoelectric hysteresis without involving any model. The main problem is its limited low frequency control performance, thus is not suitable for static nano-positioning.

The motivation of this work is to develop a high-bandwidth, low cost and real-time feedforward control scheme which does not rely on expensive computational resources to compensate the hysteretic nonlinearity. The novelties of the proposed method can be summarized as follows. First, according to the authors' best knowledge, it is the first analog-implemented feedforward controller which is able to precisely characterize asymmetric, amplitude-dependent and rate-dependent effects of the piezoelectric hysteresis. Such kind of analog implementation brings several advantages to real practice over its digital counterpart, such as low cost, no inherent bandwidth limit and high resolution due to the absence of analog-digital conversion. These advantages could be helpful for both implementation and performance improvement of nano-positioning systems. Second, to deal with the complicated rate-dependent effect, a general method of implementing curve fitting in Bode magnitude plot is proposed by using fractional order compensators (FOCs). In principle, the developed method is able to synthesize compensators or filters with arbitrarily desired magnitude shape, thus could be valuable for a wide range of applications beyond the hysteresis compensation topic of this work. Third, as a key point of the proposed method is to model and compensate the hysteretic disturbance rather than the displacement, the inverse model is easy to obtain.

The paper is organized as follows: Section II formulates the problem and gives the general idea of the proposed method. The asymmetric hysteresis modeling and validation are presented in Section III. Section IV describes the rate-dependent modeling method. Section V shows the compensation results. We conclude this work in Section VI.

II. Problem Formulation

Piezoelectric actuators can be modeled as a system in which a nonlinear subsystem connects in series with a linear time invariant (LTI) subsystem. As shown in Fig.1(a), the nonlinear part $H(\cdot)$ describes hysteresis and creep effects that inherently associated with piezoelectric materials. While the linear part $P(s)$ represents its dynamics, or more specifically resonant

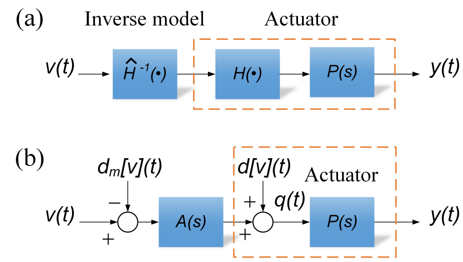

Fig. 1. Schematic diagram of (a) the commonly used hysteresis compensation strategy and (b) the proposed method

properties. This model leads to an intuitive nonlinearity compensation solution $\hat{H}^{-1}(\cdot)$, which is the inverse model of $H(\cdot)$. On the other hand, the hysteresis nonlinearity can also be treated as an internal disturbance of the plant, resulting in a disturbance-involved model of Fig.1(b). Specifically, $A(s)$ and $P(s)$ in this model denote power amplifier dynamics and the LTI part of the piezo-actuator, respectively. $d[v](t)$ is the hysteretic disturbance, while $q(t)$ is the input of the LTI system [21]. In this case, if the piezoelectric disturbance $d[v](t)$ can be precisely modeled as $d_m[v](t)$ and added into the input signal $v(t)$, a linear output displacement can be expected. It is worth noting that the term "disturbance" refers to the difference between what the system is and what it should be [22]. Therefore, the method presented in Fig.1(b) is a general solution to compensate the hysteresis effect. Considering that the creep related issues only happens at low-frequency range and have been well-investigated [23], this work will only focus on modeling and compensating the challenging hysteresis related issues. In this context, developing a complete model that could characterize the rate-dependent, amplitude-dependent and asymmetric effects of piezoelectric hysteresis becomes the primary concern, which will be detailed in the following sections.

Remark: It should be noted that due to the finite bandwidth of power amplifier, a phase shift usually exists between the input signal and the resultant displacement, especially when operating at high frequencies. As a particular case, if sinusoidal waves are chosen as the system input, then the phase shift will result in a hysteresis-like input-output relationship, even the piezoelectric hysteresis has been perfectly compensated for. Therefore, it is important to distinguish between the piezoelectric hysteresis and those of the pure phase shift. This work will only focus on the compensation of the piezoelectric hysteresis.

III. Asymmetric and Amplitude-Dependent Hysteresis Modeling and Validation

In this work, polynomials are chosen to characterize the asymmetric disturbance, due to their high modeling accuracy and ease of implementation.

A. Analog Implementation Scheme

Analog feedforward control is a high-bandwidth and low-cost solution for suppressing the hysteresis nonlinearity. However, until now almost all the feedforward controllers were

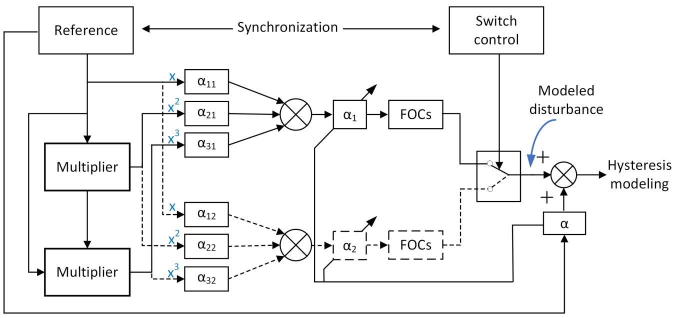

Fig. 2. Analog implementation scheme of the proposed feedforward controller.

implemented in a digital manner, primarily due to the complexity of the adopted models and their analytical inversions. As a comparison, benefiting from the simple structure of the proposed scheme, a high performance analog-implemention of the feedforward controller is available.

Fig.2 shows the general analog implementation scheme for modeling hysteresis effects. As polynomials are chosen to model the piezoelectric disturbance, several technical issues arise. The first one is on the generation of the desired polynomials. To facilitate this process without loss of generality, the reference signal was normalized to a range of 0 to 1 V. It is then multiplied several times to obtain its quadratic and cubic terms. For the purpose of minimizing the subsequent parameter identification efforts without significant degradation of the model accuracy, the polynomials is chosen to be third-order. Then the weighted sum of these three terms engenders the expected polynomials. For the reasons that will be clarified later, the constant term is not necessarily needed. In addition, because of the asymmetry, two polynomials were constructed to model the ascending and descending disturbances, respectively. The second issue is on the generation of a proper output to reproduce the hysteretic displacements. This is achieved by synchronizing the frequencies of the reference signal and the switch control signal. For example, if a sinusoidal signal is chosen as the reference, then during its ascending branch the corresponding polynomial-based disturbance model is generated. While during the descending branch, the programmable switch change to another position to pick up the corresponding polynomials. By adding the modeled disturbance into the reference, one can reproduce the asymmetric hysteresis nonlinearity. Third, the amplitude-dependent effect implies that the disturbance is dependent on the input amplitude. In order to characterize this effect, two amplitude-varying gains α_1 and α_2 are incorporated into the model, which are the functions of the input amplitude α. The next section will clarify the identification of these key parameters.

B. Polynomial Parameters Identification and Validation

The third-order polynomial estimation of disturbance has the general form of

$$\hat{d}(x) = a_0 + a_1 x + a_2 x^2 + a_3 x^3 \tag{1}$$

To obtain a continuous switch between ascending and descending disturbance models, the boundary condition of (1) should satisfy

$$\hat{d}(x)\Big|_{x=0} = 0,\ \hat{d}(x)\Big|_{x=1} = 0 \tag{2}$$

which yields

$$a_0 = 0, a_3 = -a_1 - a_2 \tag{3}$$

Therefore, the constant term of the polynomial is not necessary. Let x_i, d_i denote the sampled input (triangular signal) and output (measured disturbance) respectively, $\hat{d}_i$ denotes the estimated disturbance $(x_i, d_i, \hat{d}_i \in [0,1], i = 1, 2...n)$ and n is the number of experimental data points. Then the problem can be formulated to find the optimal coefficient $a_i (i = 1, 2, 3)$ by solving the unconstrained optimization problem of

$$min \sum_{i=1}^{n} [d_i - \hat{d}_i]^2 = min \sum_{i=1}^{n} [d_i - (a_1 x_i + a_2 x_i^2 - (a_1 + a_2) x_i^3)]^2 \tag{4}$$

The solution a = $[a_1\ a_2]$' should satisfy the following equation

$$\begin{bmatrix} \sum\limits_{i=1}^{n} (-x_i + x_i^3)^2 & \sum\limits_{i=1}^{n} (-x_i^2 + x_i^3)(-x_i + x_i^3) \\ \sum\limits_{i=1}^{n} (-x_i^2 + x_i^3)(-x_i + x_i^3) & \sum\limits_{i=1}^{n} (-x_i^2 + x_i^3)^2 \end{bmatrix} \cdot \begin{bmatrix} a_1 \\ a_2 \end{bmatrix} = \begin{bmatrix} \sum\limits_{i=1}^{n} (x_i - x_i^3) d_i \\ \sum\limits_{i=1}^{n} (x_i^2 - x_i^3) d_i \end{bmatrix} \tag{5}$$

By substituting a_1 and a_2 into (3), the optimally fitted polynomial can be found.

The amplitude-dependent effect, however, poses another challenge on precisely modeling the hysteresis behavior. Instead of identifying the disturbance model at given amplitudes, a simplified strategy is proposed where only the full stroke disturbance model is developed. We then use this model and an amplitude-varying gain to optimally approximate the disturbance at different amplitudes, in a sense of least square error.

Note that if we use $\hat{y}_i$, $\tilde{y}_i$ and y_i to represent the estimated displacement, reference displacement and the measured displacement, then

$$\hat{y}_i = \tilde{y}_i + \hat{d}_i \tag{6}$$

$$y_i = \tilde{y}_i + d_i \tag{7}$$

Therefore, the percentage root-mean-square (RMS) error of the displacement estimation can be defined as

$$\begin{aligned} e_{rms}(\%) &= \frac{\sqrt{\frac{1}{N} \sum\limits_{i=1}^{n} (\hat{y}_i - y_i)^2}}{\max(y_i) - \min(y_i)} \times 100\% \\ &= \frac{\sqrt{\frac{1}{N} \sum\limits_{i=1}^{n} (\hat{d}_i - d_i)^2}}{\max(y_i) - \min(y_i)} \times 100\% \end{aligned} \tag{8}$$

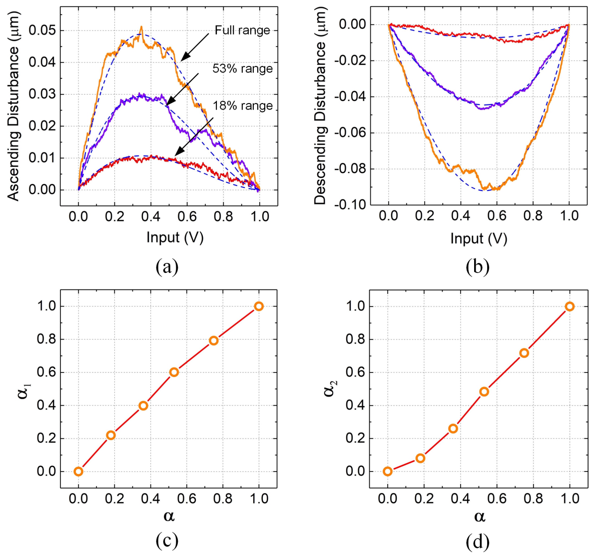

Fig. 3. Polynomial-based model of (a) ascending and (b) descending piezoelectric disturbances for different amplitudes. (c) The identified relationship between the input amplitude α and the ascending disturbance amplitude α_1. (d) The relationship between the input amplitude α and the descending disturbance amplitude α_2.

This is essentially equivalent to the objective function of (4), meaning that the identified polynomials will have an optimal RMS error.

Experimental validation of the proposed method was conducted using a custom-built high-bandwidth nanopositioner, which is detailed in Section V. To ease the comparison between the measurement and the estimation, we normalize the amplitude of the measured displacement to unity. The reference signal i.e. controller input was a triangular wave, with a frequency of 1 Hz. As shown in Fig.3 (a) and (b), the ascending and descending disturbances at full stroke were identified as $\hat{d}_a = 0.3546x - 0.6433x^2 + 0.2887x^3$ and $\hat{d}_d = -0.2398x + 0.0838x^2 + 0.156x^3$, respectively. The amplitude-varying gains α_1 and α_2 were then found using these two models, as shown in Fig.3(c) and (d). It is observed that the nonlinear relationship between α_1, α_2 and α mainly locates in the region where the input amplitude is small, typically less than half of the full input range.

C. Simplified Disturbance Approximation Using Sinusoidal Signals

The asymmetric hysteresis model can be simplified by using sinusoidal signals, in which case the number of parameters that needs to be identified reduced from 3 to only 1 for each branch, and thus further streamlines the system configuration. Specifically, two sinusoidal signals are adopted to approximate the ascending and descending disturbances. By calculating a proper amplitude of each sine wave, it is found that a good approximation can also be achieved. The amplitude that needs to be determined is the solution of the following problem

$$min \sum_{i=1}^{n} \left[d_i - A\sin(\pi x_i)\right]^2 \tag{9}$$

where d_i and x_i have the same definition as in (4). The sinusoidal signal $\hat{d}(x) = Asin(\pi x)$ satisfies the boundary condition of (2). By solving this simple optimization problem, the amplitude A can be determined as

$$A = \frac{\sum_{i=1}^{n} d_i \sin(\pi x_i)}{\sum_{i=1}^{n} \sin^2(\pi x_i)} \tag{10}$$

It should be noted that polynomial-based estimation has a better precision and can be easily extended for modeling other kinds of hysteretic nonlinearities. While for the sine-wave-based estimation, it is only suitable for modeling the disturbances that has similar shapes, such as the piezoelectric hysteresis disturbance.

IV. Rate-dependent Effect Modeling and Validation

A. Modeling Principle

Rate-dependent effect of hysteresis essentially indicates that the magnitude of the disturbance varies with the operating frequencies. Therefore, to precisely characterize this effect, compensators or filters with arbitrary shapes in Bode magnitude plot are necessary. This is the most challenging issue of the controller design. To deal with this, the proposed solution is to implement curve fitting in Bode magnitude plot, meaning that one needs to first find the interested interpolation points and then achieve arbitrarily desired slope when necessary. This process can be divided into the following three steps:

Step 1: Choose N frequencies of interest and identify the polynomial coefficients at each frequency for disturbance estimation. The identified polynomial $\hat{p}_1$ at the lowest frequency will serve as a basis for the following steps.

Step 2: Find proper gains $K_i (1 < i <= N)$ which minimize the difference between the i th polynomial $\hat{p}_i$ and the basis one $\hat{p}_1$. In this way, the estimated disturbance at different frequencies can be represented by a basis function times a varying gain.

Step 3: Choose the frequency points that can capture the general trend of rate-dependent effect, and implement curve fitting using the identified gain of these points. This is achieved by designing a FOC between the neighboring frequencies and connecting all of these compensators in series to complete the design. Note that to simplify the design, the points used to design FOCs is generally less than the identified points in step 1.

As the issue of polynomial identification has been fully solved in previous section, we now proceed to the process of step 2 to find the gains K_i. This is similar to the problem of (9), i.e. solving the optimization problem of

$$min \sum_{k=1}^{n} \left[\hat{p}_{1k} - K_i \hat{p}_{ik}\right]^2 \tag{11}$$

where

$$\begin{gathered}\hat{p}_{ik} = a_{i1}x_k + a_{i2}x_k^2 + a_{i3}x_k^3 \\ (x_k \in [0,1], i = 2 \cdots N, k = 1 \cdots n)\end{gathered} \tag{12}$$

Hence,

$$K_i = \frac{\sum_{k=1}^{n} \hat{p}_{1k}\hat{p}_{ik}}{\sum_{k=1}^{n} \hat{p}_{ik}^2} \tag{13}$$

It is worth pointing out that sine-wave-based disturbance approximation can also be used in steps 1 and 2, which actually makes the parameter identification and gain finding processes easier. In this case each K_i is simply a ratio between corresponding amplitudes.

Once K_i is obtained, the compensator design proceeds to step 3. Fractional order compensators are part of recently developed fractional order control theories [24], which have a general form of

$$G(s) = \left(\frac{\lambda s + 1}{x\lambda s + 1}\right)^{\beta} \tag{14}$$

where β is not an integer but a rational or even an irrational number. Therefore, different from classical compensators, the slope of the magnitude curve in a Bode plot is not an integer times of ± 20 dB/dec, but $\pm 20\beta$ dB/dec. This is actually the most interesting feature of the FOC for this work, since the slope of the compensator magnitude can be arbitrarily designed by choosing β.

Suppose N frequency points of interest have been determined from step 1 and $N-1$ gains K_i are ready from step 2 (the gain of the basis function is one). Then $N-1$ FOCs connected in series need to be designed so that the resultant compensator will pass through the control points. The compensator $G_f(s)$ can be written as

$$G_f(s) = \left(\frac{\lambda_1 s + 1}{x_1\lambda_1 s + 1}\right)^{\beta_1} \cdots \left(\frac{\lambda_{N-1} s + 1}{x_{N-1}\lambda_{N-1} s + 1}\right)^{\beta_{N-1}} \tag{15}$$

By taking the common logarithm of each side, we have

$$\begin{aligned} \log|G_f(j\omega)| = \beta_1 \log\left|\frac{j\lambda_1\omega + 1}{jx_1\lambda_1\omega + 1}\right| + \cdots + \beta_{N-1} \\ \cdot \log\left|\frac{j\lambda_{N-1}\omega + 1}{jx_{N-1}\lambda_{N-1}\omega + 1}\right| \end{aligned} \tag{16}$$

Furthermore, $G_f(s)$ will pass through $N-1$ interpolation points, meaning that

$$|G_f(j\omega)|_{\omega=\omega_i} = K_i \ \ (2 \le i \le N) \tag{17}$$

Substituting (17) into (16) gives a set of linear equations

$$\begin{aligned} \log|g_i| = \beta_1 \log\left|\frac{j\lambda_1\omega + 1}{jx_1\lambda_1\omega + 1}\right|_{\omega=\omega_i} + \cdots + \beta_{N-1} \\ \cdot \log\left|\frac{j\lambda_{N-1}\omega + 1}{jx_{N-1}\lambda_{N-1}\omega + 1}\right|_{\omega=\omega_i} \ (2 \le i \le N) \end{aligned} \tag{18}$$

By solving these $N-1$ equations, the FOC order β_i can be determined.

The next issue is to convert the FOC into its integer equivalent so that it can be properly implemented by analog circuits. Due to the efforts of fractional order control community, several convenient toolboxes have been developed, such as CRONE, Ninteger and FOMCON [25]. In this work, FOMCON is adopted to complete the necessary conversion.

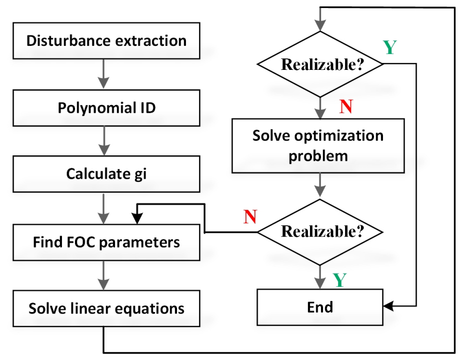

Fig. 4. Flow chart of modeling rate-dependent effect by designing FOCs.

TABLE I
OPTIMAL GAIN K_i AT DIFFERENT FREQUENCIES

Frequency	20 Hz	40 Hz	60 Hz	80 Hz	100 Hz
K_i	1.1	1.07	1.04	1.09	1.17

Theoretically, the curve fitting approach presented above is able to ensure the magnitude shape as desired. However, for the cases where the magnitude varies dramatically in a narrow frequency range, the order of the compensator would be very large. This will lead to a significant amount of errors to happen in both FOC to normal transfer function conversion and the practical implementation. To deal with this problem, constraints on the order of the FOC needs to be considered. In this case, the curve fitting issue turns to find proper orders that minimize the fitting errors, i.e.

$$\begin{aligned} min \sum_{i=1}^{N-1}\left(\sum_{j=1}^{N-1}\beta_j \log\left|\frac{j\lambda_i\omega + 1}{jx_i\lambda_i\omega + 1}\right|_{\omega=\omega_j} - \log|K_{i+1}|\right)^2 \\ s.t.\ 0 < \beta_i \le c_i \ \ (i = 1 \cdots N-1) \end{aligned} \tag{19}$$

where c_i represents the upper bound of the FOC order. A detailed flow chart is shown in Fig.4 to clarify the procedure of designing FOCs for characterizing the rate-dependent effect.

B. FOCs Design and Validation

To characterize the rate-dependent disturbance from 1 Hz to 100 Hz, a series of experiments were conducted. The disturbances were extracted from the resulting displacement and presented with their polynomial-based approximations in Fig.5. The ascending disturbances, as shown in Fig.5(a1), are almost the same in the frequency range of interest. Therefore, they are considered to be static, meaning that FOCs are not necessarily needed. However, on the other hand, obvious variations can be observed from the measured descending disturbances. Fig.5(b1)-(b3) present the descending disturbances at 20 Hz, 60 Hz, and 100 Hz, respectively. By following the proposed procedure, a set of optimal gain K_i can be determined according to (13), and are provided in Table I.

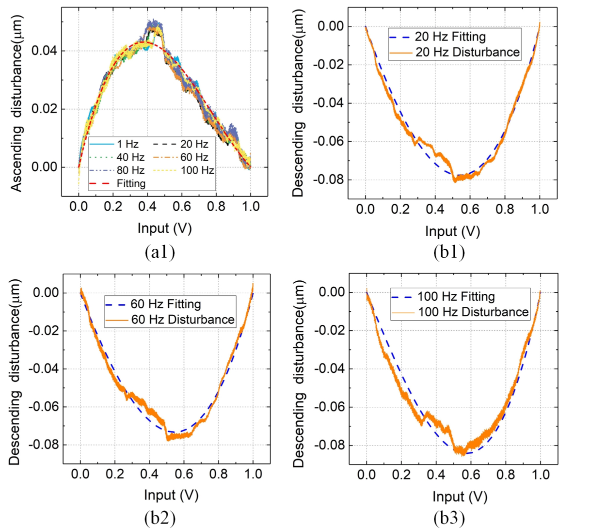

Fig. 5. (a1) Ascending disturbances and the corresponding polynomial-based model. (b1)-(b3) are descending disturbances and corresponding models at 20 Hz, 60 Hz and 100 Hz.

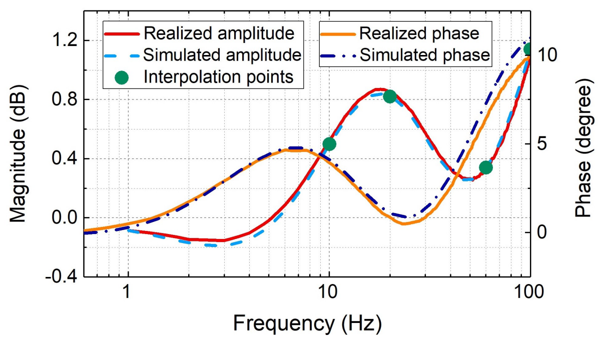

Fig. 6. Frequency response of the FPAA-implemented FOCs.

To simplify the FOCs design, we first choose gains at 20 Hz, 60 Hz and 100 Hz as interpolation points, with a starting frequency of 1 Hz. However, it turns out that the gain of the resultant FOCs at 10 Hz is close to 1.4 dB, which is unreasonably large. We therefore measure the disturbance at 10 Hz and add another interpolation point at this frequency (with a gain of 1.06). By setting the parameters of (14) and solving 4 linear equations of (18), the orders of FOCs are determined as [β_1 β_2 β_3 β_4]'= [-0.0373 0.9091 1.0418 1.8918]'. The Bode plot of the FOCs is plotted in Fig.6, showing the curve fitting results. More details on analog implementation of the designed FOCs will be discussed in the next section.

V. Experimental Setup and Compensation Performance

A. Experimental Setup

1) Nanopositioner: The experiments were conducted on a custom-built high-bandwidth nanopositioner, as shown in Fig.7(a). This nanopositioner has a stacked structure, in which three small piezo-actuators (NAC2012, Noliac) are embedded into the carefully designed flexures. The displacement of

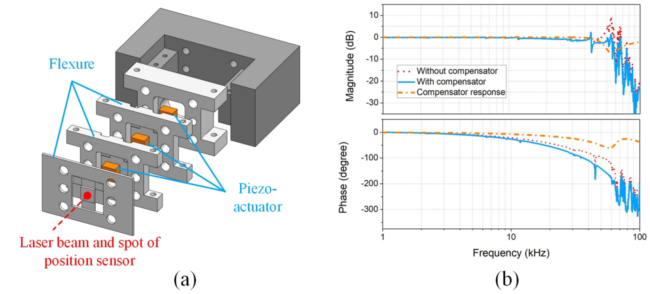

Fig. 7. (a) Exploded-view of the custmo-built nanopositioner. (b) Frequency response of the nanoposition with and without using damping compensator.

the nanopositioner was measured by a laser interferometer position sensor (SP-S 120, SIOS), showing that the full stroke is 6.92 μm. A Techproject voltage amplifier, which is dedicated to high-bandwidth nanopositioning [26] [27], was used in the experiments. Fig.7(b) plots the frequency response of the nanopositioner, indicating that the dominant resonance mode locates at 65.1 kHz. In the following experiments, the nanopositioner is driven over a wide bandwidth up to 5 kHz. This is actually a fundamental requirement for video-rate atomic force microscopy imaging with a proper resolution. To this end, resonance peaks needs to be damped. A dedicated damping compensator for achieving this was designed, with a transfer function of

$$G(s) = \frac{0.86(s^2 + 9.854 \times 10^4 s + 1.67 \times 10^{11})}{s^2 + 1.917 \times 10^5 s + 1.436 \times 10^{11}} \tag{20}$$

The performance of this damping compensator is shown in Fig.7(b), the main resonance peak and other peaks at higher frequencies have been fully damped. Although there exists a small fluctuation around 45 kHz, its impact on control performance is negligible.

2) Controller implementation: The polynomials used for modeling the hysteresis disturbance are generated by several AD835 multipliers. Besides, the majority part of the controller implementation, including amplitude-varying gain implementation, FOCs realization, programmable switch control and compensation signal generation, are achieved by using field programmable analog array (FPAA) technique (AN231K04-QUAD4, Anadigm).

The amplitude-varying gains are realized by using the voltage controlled variable gain module of FPAA. To implement the desired FOCs, the first step is to convert it to a series of integer order compensators, with the aid of FOMCON toolbox. Here we take the results shown in Fig.5 and Fig.6 as an example. The resulting FOCs are converted to a bunch of integer order compensators

$$G_1(s) = \frac{0.918(s + 48.79)(s + 14.8)}{(s + 47.49)(s + 13.99)} \tag{21}$$

$$G_2(s) = \frac{1.885(s + 107.6)(s + 63.68)}{(s + 126.4)(s + 102.2)} \tag{22}$$

$$G_3(s) = \frac{0.318(s + 380.2)(s + 221.6)}{(s + 214.9)(s + 124.8)} \tag{23}$$

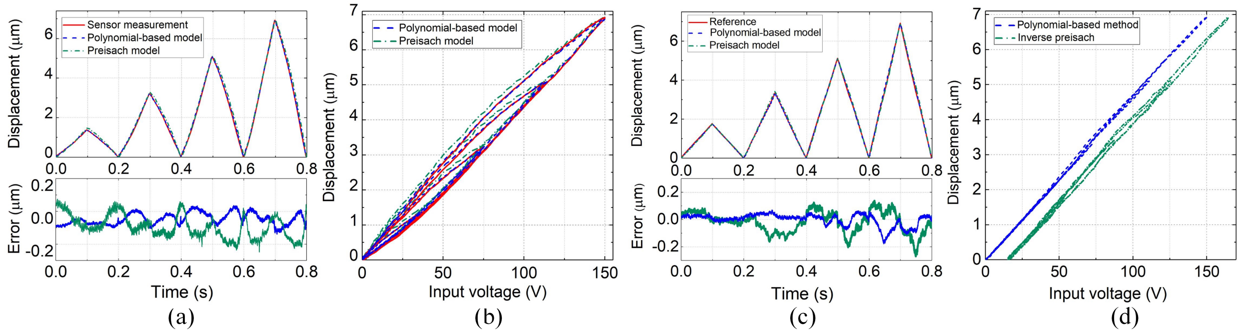

Fig. 8. (a) Hystersis modeling and the corresponding errors using Preisach model and polynomial-based model. (b) Hysteresis loop. (c) Compensation performance and the corresponding errors. (d) Linearized displacement.

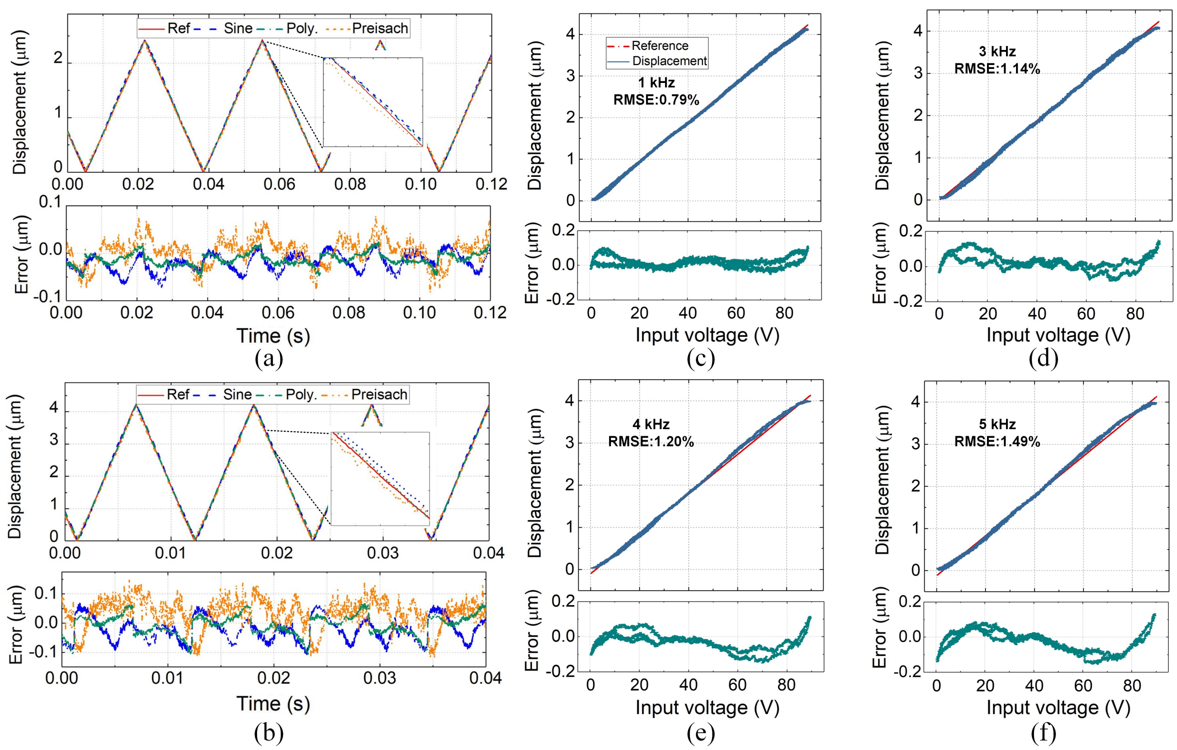

Fig. 9. Triangular trajectory tracking results at (a) 30 Hz with 50 V_{p-p} input and (b) 90 Hz with 95 V_{p-p} input. (c)-(f) are linearized displacement at 1 kHz, 3 kHz, 4 kHz and 5 kHz, and corresponding tracking errors, using inverse polynomial model.

$$G_4(s) = \frac{2.628(s+400)(s+365.6)}{(s+625.1)(s+589.4)} \tag{24}$$

They are then implemented in FPAAs based on a series of FilterBilinear blocks. The Bode plot of the simulated FOCs response is also provided in Fig.6, indicating a good match between the simulation and the real performance. It is worth noting that a phase lead which is less than 10 degree is introduced by the FOCs. However, in practice the effect of this small phase shift can be safely neglected.

B. Trajectory Tracking Performance Evaluation and Comparison

The performance of both polynomial and sinusoidal disturbance model, as proposed in Section III are evaluated experimentally. In addition, comparative studies between Preisach model and the proposed approach are also conducted. All of evaluations are in terms of modeling and compensation performance. In the Preisach model, the discretization level is chosen as $L = 200$, which is sufficiently large to characterize the hysteresis behavior of piezo-actuator [16] [28]. Thus, the total number of operators is $L(L+1)/2 = 20100$. The weight of each operator is calculated according to [29], using the MATLAB routine $lsqnonneg$ [16]. As for the hysteresis compensation, the inverse Preisach model is constructed using the method shown in [30]. The tracking performance of these approaches are now presented as follows.

1) Asymmetric and amplitude-dependent effect modeling and compensation: Triangular signal with increasing amplitude and fixed frequency at 5 Hz were adopted to evaluate the performance of the proposed method. The sensor measurement result along with the predictions by the Preisach model and polynomial-based model are shown in Fig.8(a). It is observed that the RMS error of the proposed method is 0.05 μ m, i.e. 0.7% of the motion range. While for the Preisach model, the modeling error is found to be 0.13 μm, corresponding to 1.9% of the full range. Fig.8(b) illustrates the predicted and the measured hysteresis loop, indicating that the proposed method can precisely model the asymmetric and amplitude-dependent effects of both minor and major loops. The hysteresis compensation performance is given in Fig.8(c), generally the RMS error of compensation is similar to the modeling error, which is 0.06 μm and 0.15μm,respectively. According to Fig.8(d), the displacement of the nanopositioner has been significantly linearized. Note that the Preisach compensation result is shifted to the right for the sake of clarity.

2) Frequency-dependent effect compensation: Experimental validations aiming to verify the control performance on frequency-dependent effect were conducted in a wide bandwidth, in which both polynomials and sinusoids were employed to approximate the hysteresis disturbance. It is well known that classical Preisach models can only describe the static hysteresis nonlinearity. Therefore in our studies and for the purpose of making a fair comparison, we identify the weights of relay operators at each given frequency. The results of tracking triangular trajectories at 30 Hz and 90 Hz are shown in Fig.9 (a) and (b). In Fig.9(a) a $50V_{p-p}$ voltage was applied to the nanopositioner, leading to a motion range of 2.43 μm. When using polynomial-based method, the RMS error is 0.017 μm, i.e. 0.70% of the motion range. While for sinusoid-based method, the RMS tracking error is 0.031 μm, i.e. 1.28% of the motion range. As for the Preisach model, the tracking error is 0.041 μm, corresponding to 1.69% of the motion range. We then increased the voltage applied to the nanopositioner to $95V_{p-p}$, with a operating frequency at 90 Hz. This leads to a 4.25 μm motion range. The RMS tracking error of polynomial-based method, sinusoid-based method and inverse Preisach model are 0.035 μm, 0.059 μm and 0.082 μm, as shown in Fig.9(b). Therefore, it is clear that the tracking performance of the proposed polynomial-based method is much better than the inverse Preisach approach. Note that although the performance of sinusoid-involved scheme is inferior to the polynomial-based method, it is still slightly better than the inverse Preisach model. More detailed tracking results from 1 Hz to 100 Hz using polynomial and sinusoid as disturbance models are presented in Table II, where the amplitude of voltage applied to the nanopositioner is fixed to $90V_{p-p}$. According to this table, the percentage RMS error can be down to 0.56%. Not only this, analog implementation results in a wide bandwidth of the controller. We therefore operate the nanopositioner up to 5 kHz. Fig.9(c)-(f) illustrate the compensated displacement at 1 kHz, 3 kHz, 4 kHz and 5 kHz. To clarify the piezoelectric hysteresis compensation performance, the phase lag introduced by the amplifier has been eliminated. The percentage tracking error at each frequency is 0.79%, 1.14%,1.20% and 1.49%, respectively. The tracking results at other frequencies can also be found in Table II. It is worth noting that the interpolation

TABLE II
RMS ERRORS OF TRACKING TRIANGULAR SIGNAL AT DIFFERENT FREQUENCIES USING SINE-WAVE (SW) BASED AND POLYNOMIAL (PN) BASED DISTURBANCE COMPENSATION.

Freq.(Hz)	SW(%)	PN(%)	Freq.(Hz)	PN(%)
1	0.91	0.98	200	0.85
10	0.96	0.82	400	1.02
20	0.93	0.56	600	1.08
30	1.09	0.59	800	0.95
40	1.16	0.60	1000	0.79
50	0.95	0.72	1500	1.32
60	1.17	0.66	2000	1.53
70	0.99	0.74	2500	1.38
80	1.03	0.86	3000	1.14
90	0.98	0.83	4000	1.20
100	0.78	0.56	5000	1.49

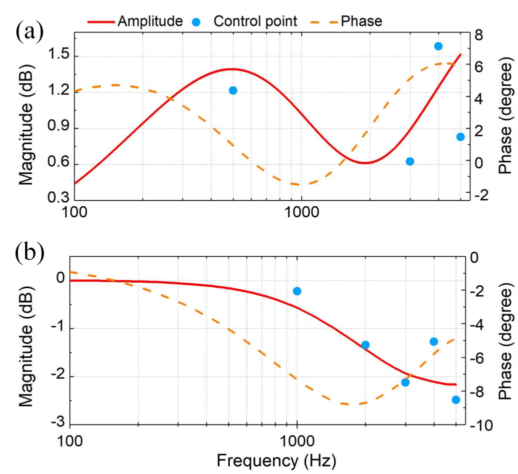

Fig. 10. Frequency response of the designed FOCs for characterizing (a) ascending and (b) descending disturbances at high frequencies.

points, as given in Fig.10, show a significant change around 4 kHz. As a result, solving equations of (18) yields FOCs with orders more than 100, thus making them not practically implementable. In this case, the strategy described in (19) is adopted and the maximum order is limited to 5. Fig.10(a) and (b) show the frequency response of the designed FOCs for modeling ascending and descending disturbances, respectively.

3) Complex trajectory tracking: To further evaluate the effectiveness of the proposed method, experiment of tracking a complex input signal defined by $u(t) = 0.415 + 0.23*(sin(2\pi t)+0.3sin(\pi t)+0.5sin(0.2\pi t))$ was conducted. Fig.11(a) shows the results of polynomial-based model, those of Preisach model and the laser interferometer measurements. It is observed that the proposed model can predict the hysteresis behavior of the nanopositioner with high accuracy. This is further demonstrated by the hysteresis loop shown in Fig.11(b). The insert picture indicates that the percentage modeling errors of polynomial-based method and Preisach model are 1.65% and 4.11%, respectively. Fig.11(c) illustrates the linearized displacement of two methods. The tracking error

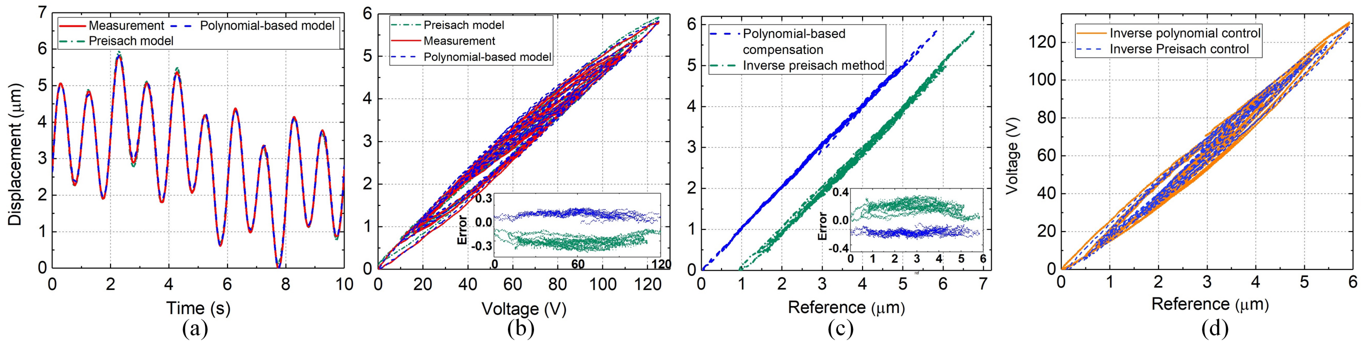

Fig. 11. (a) Modeling results of polynomial-based method and Preisach model with complex sinusoidal input. (b) Hysteresis loop, corresponding modeling errors and control voltage. (c) Linearized displacement and the tracking errors. (d) Control voltage generated from two models.

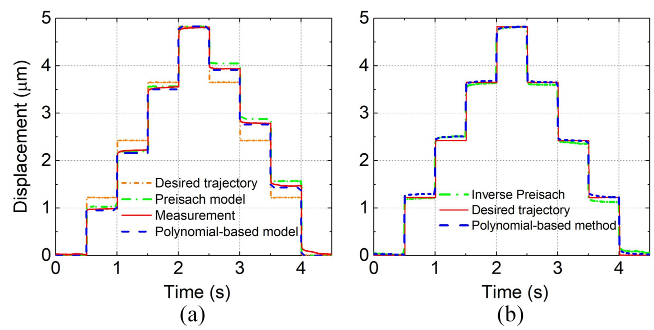

Fig. 12. (a) Desired placement, sensor measurement, Preisach model prediction and polynomial-based model prediction results. (b) Compensation results of inverse Preisach model and inverse polynomial-based model.

of two methods are 2.19% and 4.62% of the motion range. Addtionally, we also provide the control voltage generated by the inverse polynomial model and the inverse Preisach model, as swhon in Fig.11(d).

C. Further Discussions

1) On stair-like trajectory tracking: Stair-like trajectory tracking can be considered as a simplified version of typical tracking problem, since the disturbance modeling and compensation happens at finite points. However, one first needs to identify the parameters of Fig.2 using typical signals such as sinusoids or triangular waves. Once the model of disturbance is available, the modeling and compensation procedure becomes straightforward. Fig.12(a) presents the desired displacement, sensor measurement, Preisach model prediction and Polynomial-based model prediction, when applying a stair-like input voltage to the nanopositioner. The resultant asymmetric response is the outcome of hysteresis effect. Here, we still use the identified polynomials as disturbance model. After compensation, as shown in Fig.12(b), most of the hysteresis nonlinearity has been eliminated. The tracking error is found to be 2.15% for the polynomial-based model and 2.7% for the inverse Preisach model.

2) Load effect on hysteresis modeling: The payload applied to piezo-actuator or nanopositioner might significantly affect the shape of the hysteresis loop and thus posing more challenges on modeling and compensation procedures. Here we group all kinds of load into three categories: constant load, linearly dynamic load and nonlinear load. The constant load will cause a compression of the actuator, leading to a change of zero position. However, it has no effect on the shape of hysteresis loop and therefore will not affect the identified model. Second, linearly dynamic load with large stiffness will lead to the reduction of motion range. However the disturbance model and the identified relationship between α, α_1 and α_2 remains the same. In this case, the new hysteresis model can be directly obtained by taking only part of identified parameters shown in Fig.3(c) and (d), without changing other parts of the existing model. For example, if the full stroke reduces to 80%, then we only need to use the area where $\alpha \leq 0.8$ in Fig.3(c) and (d). By normalizing α, α_1 and α_2 to 1, the new model is ready to use. As for the third case, nonlinear load might lead to both stroke reduction and the change of hysteresis disturbance. In this case, it is recommended to directly identify the model in the presence of the nonlinear load, since modifying the existing model may not be helpful.

3) Analog implementation versus digital implementation: Considering that this is a comprehensive topic, we will only focus on implementation issues of the Preisach model on field programmable gate array (FPGA) for high-bandwidth control. Generally speaking, the limitations come from two aspects. First, there exists an intrinsic tradeoff among the logic resources on FPGA, the clock rate (f_{cf}), the signal frequency (f_s), the number of weights for Preisach model (N_w) and the number of points for each signal cycle (N_c). Specifically, we take the myRIO-1900 FPGA from National Instruments as an example, which has 4400 slices logic resource and 500 kHz sampling rate. The multipliers are pipelined so that it can return a result at each clock cycle. When using N multipliers, the above-mentioned parameters relate each other as follows

$$N * f_{cf} = f_s * N_w * N_c \tag{25}$$

In practice, the first issue of implementation is to reduce the total number of relay operators from 20100 to an implementable amount. This was achieved by keeping only the "active" operators, i.e. the ones with non-zero weights, which is equal to 1451. Furthermore, by using the 40 MHz onboard clock, setting $f_s = 100$ Hz and assuming only one multiplier is employed ($N = 1$), we end up with 275 points per cycle, corresponding to a 25 nm resolution. The maximum number of 16 bits multipliers available on myRIO FPGA is 5. As a consequence, the maximum operating frequency with the same resolution is limited to approximately 500 Hz. If both the desired signal frequency and the resolution needs to be improved, then the required logic resources will increase substantially, leading to a dramatic raise of the cost. Second, the sampling rate and update rate of A/D and D/A converters need to match the requirement of high-bandwidth control. For the example shown above, the minimum sampling rate needs to be 1.4 MHz when operating the nanopositioner at 5 kHz, let alone increasing the number of points per cycle for resolution improvement. Considering that typical NI FPGA only offers sampling rate up to 1 MHz, extra cost is therefore unavoidable for specialized IO modules. These two requirements could easily raise the total cost of digitally-implemented control system to a very high level. As a comparison, the cost of analog controller is not sensitive to the increase of the bandwidth, which is the most significant advantage of analog-implementation.

VI. Conclusion

This paper presents a novel hysteresis modeling and control method from a disturbance point of view, in which the asymmetric, amplitude-dependent and rate-dependent effects are explicitly characterized. Instead of modeling the displacement, polynomials or sinusoidal signals are directly used to model the hysteretic disturbance of the plant. Based on this, FOCs are further developed to characterize the rate-dependent effect by implementing curve fitting in the Bode magnitude plot. Upon completion of the modeling, the compensating signal is immediately available by changing the sign of the disturbance model. The subsequent comparative studies under various conditions between the Preisach model and the proposed method identify the advantages of analog-implemented controller, including high modeling and tracking performance, ease of implementation and low cost. The piezoelectric hysteresis has been significantly reduced down to 0.56% of the motion range, with a maximum trajectory tracking frequency up to 5 kHz. The bottleneck preventing the higher frequencies comes from the limited bandwidth of the voltage amplifier.

References

[1] Y. Liu, J. Yan, L. Wang, and W. Chen, "A two-dof ultrasonic motor using a longitudinal–bending hybrid sandwich transducer," *IEEE Trans. Ind. Electron.*, vol. 66, no. 4, pp. 3041–3050, 2018.

[2] G. Kwon, S.-H. Kim, M. Jeong, S.-H. Han, C.-S. Choi, S.-J. Han, J. Hong, and H. Lee, "High-speed atomic force microscope lithography using a piezo tube scanner driven by a sinusoidal waveform," *Ultramicroscopy*, vol. 109, no. 8, pp. 1052–1055, 2009.

[3] X. Wang, V. Pommier-Budinger, A. Reysset, and Y. Gourinat, "Simultaneous compensation of hysteresis and creep in a single piezoelectric actuator by open-loop control for quasi-static space active optics applications," *Control. Eng. Pract.*, vol. 33, pp. 48–62, 2014.

[4] P. K. Hansma, G. Schitter, G. E. Fantner, and C. Prater, "High-speed atomic force microscopy," *Science*, vol. 314, no. 5799, pp. 601–602, 2006.

[5] J. Deng, Y. Liu, W. Chen, and H. Yu, "A xy transporting and nanopositioning piezoelectric robot operated by leg rowing mechanism," *IEEE/ASME Trans. Mechatronics*, vol. 24, no. 1, pp. 207–217, 2019.

[6] C. Yang, R. Winkler, M. Dukic, J. Zhao, H. Plank, and G. E. Fantner, "Probing the morphology and evolving dynamics of 3d printed nanostructures using high-speed atomic force microscopy," *ACS Appl. Mater. Interfaces*, vol. 9, no. 29, pp. 24 456–24 461, 2017.

[7] P. Ge and M. Jouaneh, "Tracking control of a piezoceramic actuator," *IEEE Trans. Control Syst. Technol.*, vol. 4, no. 3, pp. 209–216, 1996.

[8] H. Habibullah, H. Pota, I. R. Petersen, and M. Rana, "Tracking of triangular reference signals using lqg controllers for lateral positioning of an afm scanner stage," *IEEE/ASME Trans. Mechatronics*, vol. 19, no. 4, pp. 1105–1114, 2014.

[9] S. Bashash and N. Jalili, "Robust adaptive control of coupled parallel piezo-flexural nanopositioning stages," *IEEE/ASME Trans. Mechatronics*, vol. 14, no. 1, pp. 11–20, 2009.

[10] Y. Jian, D. Huang, J. Liu, and D. Min, "High-precision tracking of piezoelectric actuator using iterative learning control and direct inverse compensation of hysteresis," *IEEE Trans. Ind. Electron.*, vol. 66, no. 1, pp. 368–377, 2018.

[11] D. C. Jiles and D. L. Atherton, "Theory of ferromagnetic hysteresis," *J. Magn. Magn. Mater.*, vol. 61, no. 1-2, pp. 48–60, 1986.

[12] S. Rosenbaum, M. Ruderman, T. Strohla, and T. Bertram, "Use of jiles–atherton and preisach hysteresis models for inverse feed-forward control," *IEEE Trans. Magn.*, vol. 46, no. 12, pp. 3984–3989, 2010.

[13] M. Rakotondrabe, "Bouc–wen modeling and inverse multiplicative structure to compensate hysteresis nonlinearity in piezoelectric actuators," *IEEE Trans. Autom. Sci. Eng.*, vol. 8, no. 2, pp. 428–431, 2011.

[14] Y. Liu, D. Du, N. Qi, and J. Zhao, "A distributed parameter maxwell-slip model for the hysteresis in piezoelectric actuators," *IEEE Trans. Ind. Electron.*, vol. 66, no. 9, pp. 7150–7158, 2018.

[15] Y. Liu, Y. Wang, and X. Chen, "Online hysteresis identification and compensation for piezoelectric actuators," *IEEE Trans. Ind. Electron.*, 2019.

[16] Z. Li, J. Shan, and U. Gabbert, "Development of reduced preisach model using discrete empirical interpolation method," *IEEE Trans. Ind. Electron.*, vol. 65, no. 10, pp. 8072–8079, 2018.

[17] L. Chuntao and T. Yonghong, "A neural networks model for hysteresis nonlinearity," *Sens. Actuators A Phys.*, vol. 112, no. 1, pp. 49–54, 2004.

[18] M. Al Janaideh, S. Rakheja, and C.-Y. Su, "Experimental characterization and modeling of rate-dependent hysteresis of a piezoceramic actuator," *Mechatronics*, vol. 19, no. 5, pp. 656–670, 2009.

[19] A. Fleming and K. Leang, "Charge drives for scanning probe microscope positioning stages," *Ultramicroscopy*, vol. 108, no. 12, pp. 1551–1557, 2008.

[20] C. Yang, C. Li, F. Xia, Y. Zhu, J. Zhao, and K. Youcef-Toumi, "Charge controller with decoupled and self-compensating configurations for linear operation of piezoelectric actuators in a wide bandwidth," *IEEE Trans. Ind. Electron.*, vol. 66, no. 7, pp. 5392–5402, 2019.

[21] J. Yi, S. Chang, and Y. Shen, "Disturbance-observer-based hysteresis compensation for piezoelectric actuators," *IEEE/ASME Trans. Mechatronics*, vol. 14, no. 4, pp. 456–464, 2009.

[22] Z. Gao, "On the centrality of disturbance rejection in automatic control," *ISA transactions*, vol. 53, no. 4, pp. 850–857, 2014.

[23] H. Jung and D.-G. Gweon, "Creep characteristics of piezoelectric actuators," *Rev. Sci. Instrum.*, vol. 71, no. 4, pp. 1896–1900, 2000.

[24] C. A. Monje, Y. Chen, B. M. Vinagre, D. Xue, and V. Feliu-Batlle, *Fractional-order systems and controls: fundamentals and applications*. Springer Science & Business Media, 2010.

[25] Z. Li, L. Liu, S. Dehghan, Y. Chen, and D. Xue, "A review and evaluation of numerical tools for fractional calculus and fractional order controls," *INT. J. CONTROL*, vol. 90, no. 6, pp. 1165–1181, 2017.

[26] G. Schitter, K. J. Astrom, B. E. DeMartini, P. J. Thurner, K. L. Turner, and P. K. Hansma, "Design and modeling of a high-speed afm-scanner," *IEEE Transactions on Control Systems Technology*, vol. 15, no. 5, pp. 906–915, 2007.

[27] J. D. Adams, A. Nievergelt, B. W. Erickson, C. Yang, M. Dukic, and G. E. Fantner, "High-speed imaging upgrade for a standard sample scanning atomic force microscope using small cantilevers," *Review of Scientific Instruments*, vol. 85, no. 9, p. 093702, 2014.

[28] J. Å. Stakvik, M. R. Ragazzon, A. A. Eielsen, and J. T. Gravdahl, "On implementation of the preisach model: identification and inversion for hysteresis compensation," 2015.

[29] X. Tan, R. Venkataraman, and P. S. Krishnaprasad, "Control of hysteresis: Theory and experimental results," in *Smart. Mater. Struct.*, vol. 4326, pp. 101–112, 2001.

[30] S. Xiao and Y. Li, "Modeling and high dynamic compensating the rate-dependent hysteresis of piezoelectric actuators via a novel modified inverse preisach model," *IEEE Trans. Control Syst. Technol.*, vol. 21, no. 5, pp. 1549–1557, 2012.